

## Hydrogen Micro Pores and Their Affects on Mechanical Properties

Hiroyuki Toda<sup>1</sup>, Kentaro Uesugi<sup>2</sup>, Yoshio Suzuki<sup>2</sup> and Masakazu Kobayashi<sup>1</sup>

<sup>1</sup>Department of Production Systems Engineering, Toyohashi University of Technology, 1-1, Hibarigaoka, Tempaku, Toyohashi, AICHI 441-8580, Japan

<sup>2</sup>Japan Synchrotron Radiation Research Institute, 1-1-1 Kouto, Sayo, HYOGO 679-5198, Japan

High-density micro pores have been identified to exist in almost all kinds of aluminum alloys except pure aluminum according to our extensive 3D/4D (i.e., 3D + time axis) observation with the synchrotron X-ray microtomography with recently enhanced resolution levels. Formation, growth, shrink and annihilation behaviors of each micro pore are tracked throughout heat treatments and metal forming processes. It has been clarified from 3D/4D quantitative analysis that the micro pores exhibit the Ostwald ripening during heat treatments. It has been found that considerable amount of hydrogen contained in aluminum alloys is trapped in micro pores, while it is quite limited in a pure aluminum. Local strain distribution has been visualized by tacking microstructural features in 4D, representing remarkably inhomogeneous strain distribution during rolling. It has been also clarified that there is a strong correlation between the local strain values with a variety of pore closure behaviors. Such micro pores act as a fatigue crack initiation site and fatal defects under tension. We also reports how mechanical properties of aluminum alloys are degraded due to the existence of micro pores. Especially it is noteworthy that the ductile fracture of aluminum alloys is more or less dominated by micro pore growth in addition to, or instead of the well-known void initiation/growth/coalescence process from particle damage.

**Keywords:** *microtomography; hydrogen; micro pore; ductile fracture; fatigue.*

### 1. Nucleation and growth of hydrogen micro pores

Measured hydrogen content ranges about 0.11 ~ 0.60 cm<sup>3</sup> / 100 g Al even in practical wrought aluminum alloys, which is several orders of magnitude higher than the solubility of hydrogen extrapolated from the high temperature side [1]. It is attributable to the well-known hydrogen solubility gap at the melting temperature and the existence of thin but robust surface oxide film. Supersaturated hydrogen is partitioned between interstitial solution and trap sites. Hydrogen trap sites include dislocations, vacancies, solute atoms, various precipitates and high-angle grain boundaries. It is interesting to note that supersaturated hydrogen is not readily lost during storage at room temperature, or even after a combination of high-temperature exposure and hot working during the production processes of wrought aluminum alloys. It can be easily assumed that the oxide film impedes the release of hydrogen from solid aluminum in addition to the effects of various trap sites.

Table 1 Number density and average diameter of micro pores in various aluminum alloys.

Materials	Number density (10 <sup>12</sup> /m <sup>3</sup> )	Average dia. (μm)
Al-Si-Mg die-cast	8.0	1.9
A1050	3.2	1.7
A2024	69.6	3.4
A5XXX	14.5	4.0
A6061	18.4	2.6
A7475	20.2	3.4

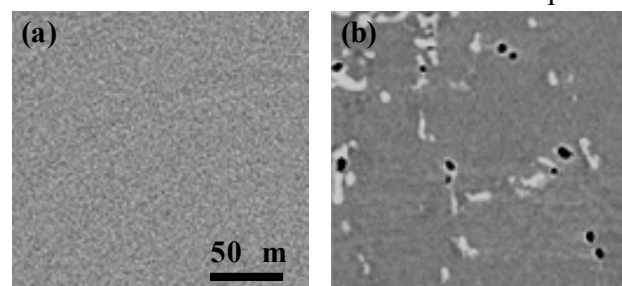


Fig.1 2D slices of reconstructed volumes, representing the existence of micro pores in many aluminum alloys. (a) an A1050 alloy and (b) an A 2024 alloy.

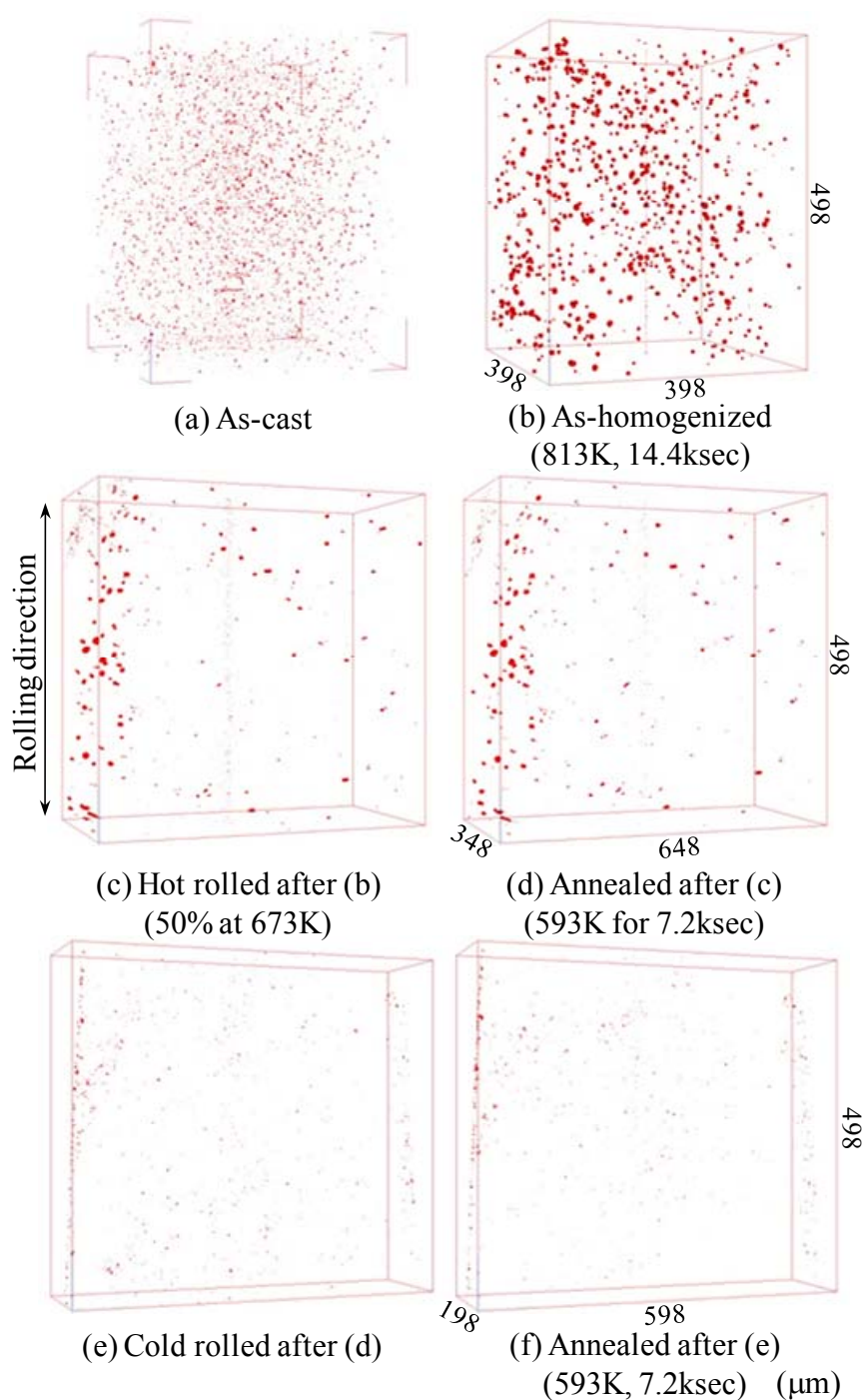


Fig. 2 3-D sequential observations of micropore distribution (red) in the rolling experiment.

high-density pores had not been recognized until the X-ray tomography was applied.

Figure 2 shows the 3D reconstructed images of micro pores in as-cast, as-homogenized and hot-and cold-rolled Al-4mass%Mg alloys [6]. Note that only micro pores are identified, whereas underlying aluminum and other phases are not displayed in the figure. In the as-cast condition, small micro pores and sometimes interdendritic shrinkage cavities are seen. It has been shown according to a 3D image analysis that at least 60 % of micro pores were formed heterogeneously on constituent particles, and there was little evidence that vacancies are involved in any way in the formation

As is well known, porosity is commonly observed in both wrought and cast aluminum alloys. Recently, the existence of high-density micro pores in wrought aluminum alloys has been revealed using the synchrotron X-ray microtomography, being a great surprise to materials scientists and engineers [2]. Summary of the micro pore observation is shown in Table 1 and Fig. 1. Porosity can therefore be characterized as another hydrogen trap site in aluminum alloys. Actual 3D images of micro pores are available in the literature for pure aluminum [3], 2024 [4,5], 5XXX [3,6] and 7075 [7] aluminum alloys and Al-Si-Mg cast alloys [2,8]. Another point to note is that high-purity aluminum, which includes industrial pure aluminum, usually shows much lower porosity for a given hydrogen content as also shown in Table 1. The X-ray microtomography technique is especially effective for micro pore observation, since micro pores are easily filled with abrasive powders during sample preparation processes for observation, such as cutting and polishing. This is the reason why such

Table 2 Estimated trap site coverage and the amount of hydrogen at each trap site.

Materials	Trap sites	Trap density, $N_T / \times 10^6$ sites/m <sup>3</sup>	Trap site occupancy, $\theta_T$	Trapped hydrogen, $\times 10^6 C_T$ /atoms H/m <sup>3</sup>
High-hydrogen-content alloy (5.12 ml/100gAl)	Interstitial	$5.85 \times 10^{22} = N_L$	$8.88 \times 10^{-5} = \theta_L$	$5.20 \times 10^{18}$
	Solute Mg atom	$1.23 \times 10^{21}$	$9.21 \times 10^{-4}$	$1.33 \times 10^{18}$
	Dislocation	$6.89 \times 10^{17}$	0.970	$6.68 \times 10^{17}$
	Grain boundary	$8.47 \times 10^{16}$	0.992	$8.40 \times 10^{16}$
	Micropore	-	-	$1.88 \times 10^{17}$
Medium-hydrogen-content alloy (4.94 ml/100gAl)	Interstitial	$5.85 \times 10^{22} = N_L$	$8.46 \times 10^{-5} = \theta_L$	$4.95 \times 10^{18}$
	Solute Mg atom	$1.23 \times 10^{21}$	$8.78 \times 10^{-4}$	$1.08 \times 10^{18}$
	Dislocation	$2.54 \times 10^{17}$	0.968	$2.46 \times 10^{17}$
	Grain boundary	$4.84 \times 10^{16}$	0.991	$4.80 \times 10^{16}$
	Micropore	-	-	$6.34 \times 10^{17}$
Low-hydrogen-content alloy (0.30 ml/100gAl)	Interstitial	$5.85 \times 10^{22} = N_L$	$1.55 \times 10^{-6} = \theta_L$	$9.07 \times 10^{16}$
	Solute Mg atom	$1.23 \times 10^{21}$	$1.61 \times 10^{-5}$	$1.98 \times 10^{16}$
	Dislocation	$1.80 \times 10^{17}$	0.357	$6.43 \times 10^{16}$
	Grain boundary	$3.71 \times 10^{16}$	0.677	$2.51 \times 10^{16}$
	Micropore	-	-	$2.23 \times 10^{17}$
99.999 % Al (0.29 ml/100gAl)	Interstitial	$6.03 \times 10^{22} = N_L$	$4.09 \times 10^{-6} = \theta_L$	$2.46 \times 10^{17}$
	Dislocation	$2.26 \times 10^{17}$	0.594	$1.34 \times 10^{17}$
	Grain boundary	-	-	-
	Micropore	-	-	$3.40 \times 10^{16}$

process of micro pores [3]. During the homogenization treatment at 813 K for 14.4 ks, small and high-density micro pores were gradually shrank and annihilated, while some micro pores were grown. This micro pore growth behavior should be consistent with the well-known Ostwald ripening mechanism, which was identified in the previous study to be predominant over the micro pore growth in aluminum alloys, and not consistent with micro pore migration/coalescence via atom transport through surface diffusion, vacancy volume diffusion or vapor transport through gas [3]. There was a marked difference in the appearance of the micro pore distribution in 99.999 % aluminum compared to the Al-Mg alloy even when total hydrogen content is similar [3]. This difference is attributable to the lack of hydrogen precipitation sites in pure aluminum. Hydrogen trapped in all the micro pores was estimated, assuming a) that a thermal equilibrium exists between surface tension and b) that the internal gas pressure in the micro pores obeys the ideal gas law. It is noteworthy that about 53 % of hydrogen was trapped within micro pores in the Al-Mg alloy with a low hydrogen content, while although the total hydrogen content was similar, it was less than 7 % in pure aluminum.

Hydrogen partitioning to the normal interstitial lattice and other trap sites was also analyzed in our previous paper as shown in Table 2 [3], revealing that micro pores are the major hydrogen trap site in the Al-Mg alloy with a low hydrogen content. It can be inferred that excess hydrogen in solid aluminum is predominantly partitioned to the micro pores, and that occupancies of other trap sites are elevated with further increases in hydrogen concentration. It has been also clarified that the rate of trap site occupancies in dislocations and grain boundaries is very high, although the absolute amount of hydrogen trapped at grain boundaries is one to two orders of magnitude smaller than that at the other trap sites. It has been reported that the formation of blisters is suppressed by applying cold deformation of 20 ~ 60% [9]. This may be consistent with the high trap site occupancies at dislocations, which are close to unity for high- and medium-hydrogen-content alloys shown in Table 2. Cold deformation inevitably leads to an increase in dislocation density, as a result of which the capacity for hydrogen storage at dislocations would be significantly expanded.

## 2. Shrinkage and annihilation of hydrogen micro pores during metal working

The majority of the micro pores disappear after hot rolling, while micro pores are to some extent residual in the peripheral layer, as seen in Fig. 2 (c). Micro pores are flattened to oblate spheroids to this extent. The application of the annealing treatment at 593 K for 7.2 ks after hot rolling gives rise to further Ostwald ripening, as has been verified in Fig. 2 (d) and (f), although its extent is limited. The subsequent cold rolling further reduces the number, size and volume fraction of micro pores.

A variety of geometrically varied behaviors are observed on closer inspection. For example, some micro pores remain even after 60 % compression, while others have been apparently annihilated. It is noteworthy that some of the annihilated micro pores are reinitiated at their original positions before annihilation, even when  $\sim 22$  % macroscopic strain is applied after their apparent annihilation, while new micro pore initiation is also identified after high-temperature exposure. These behaviors have been experimentally confirmed by tracking marker particles to obtain a local displacement field, thereby predicting a trajectory for each micro pore, even after its annihilation. The annihilation behavior of the micro pores during surface cold working has been also confirmed as shown in Fig. 3 using the synchrotron radiation microtomography [10]. Peening treatment resulted in the annihilation of most of the micro pores in the upper part of the Al-Si-Mg cast aluminum alloy. Specifically, micro pores of over  $10\ \mu\text{m}$  capable of initiating fatigue cracks were completely annihilated.

We consider the annihilation behavior of micro pores is dependent on the extent of the local plastic deformation of the aluminum matrix around them, and it varied significantly, with large pores remaining in some regions in which the apparent effective plastic strain was below 50% [6,10]. The shrinkage/annihilation behaviors of the micro pores could be interpreted as a function of local effective strain, while hydrostatic strain could not be associated with them as shown in Fig. 4 [10]. The local strain was measured in a series of tomographic volumes by tracking microstructural features [11]. The complete annihilation of large pores with the hot and cold rolling and surface cold working suggests that the application of sufficient and appropriate plastic working is effective in

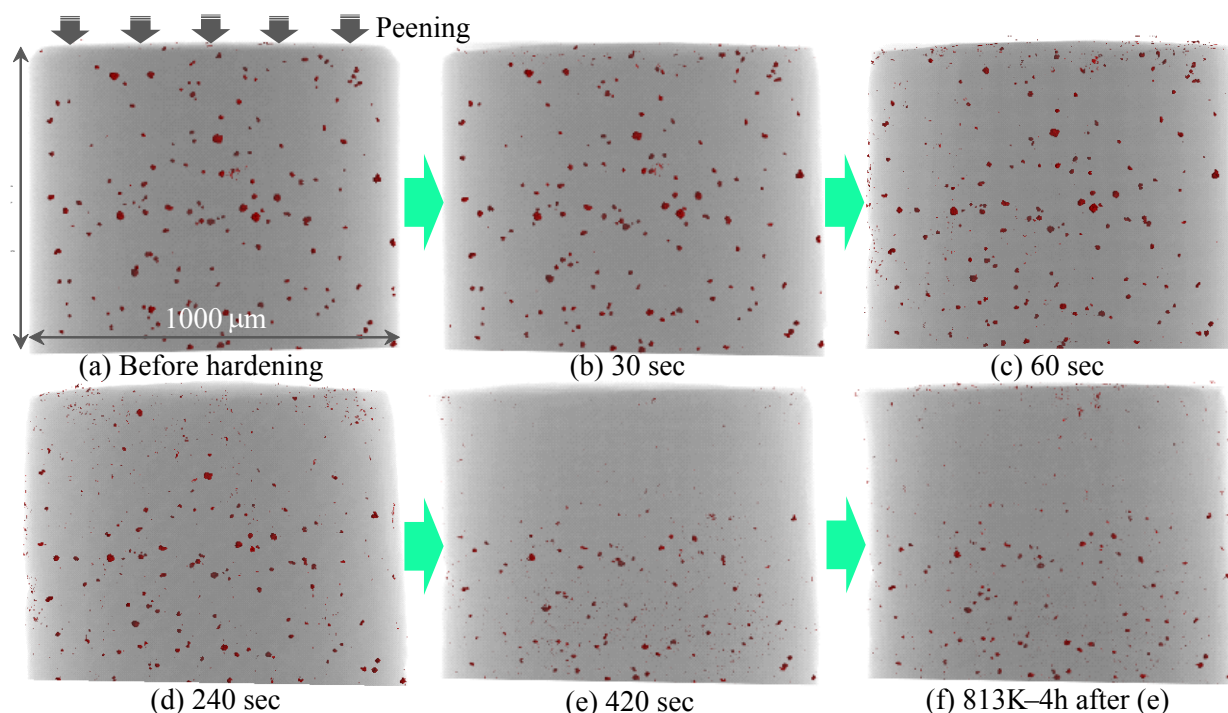
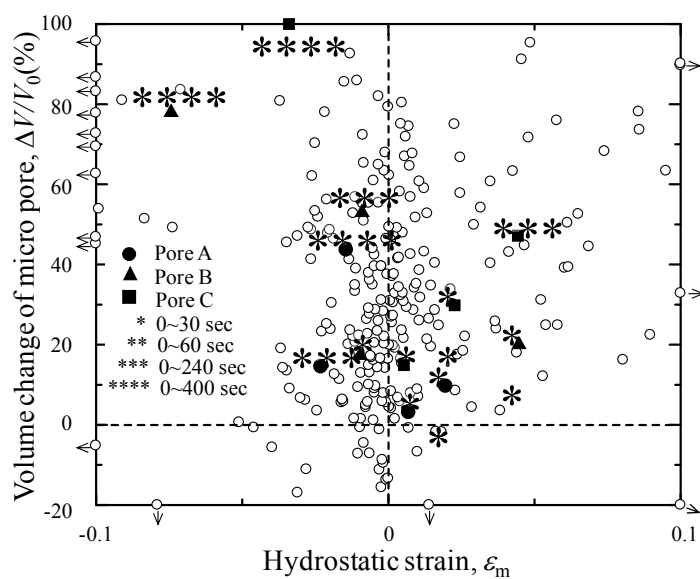
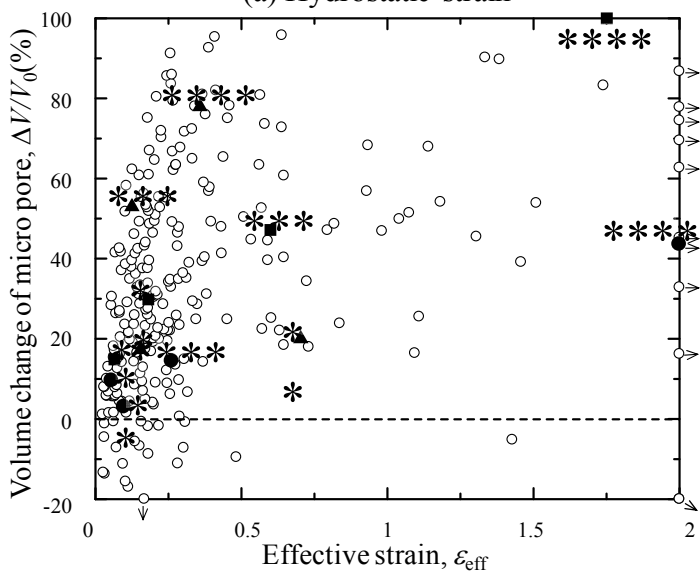


Fig. 3 3D perspective views of the tomographic specimen, representing the change in micro pore distribution during the surface hardening and subsequent heat treatment in an Al-6.8Si-0.4Mg cast aluminum alloy. Only the micro pores have been extracted and superposed on translucent specimen images.



(a) Hydrostatic strain



(b) Effective strain

Fig. 4 Relationships between shrinkage behaviors of micro pores and local strain components around micro pores, representing the dominant factor for pore closure. (a) hydrostatic strain, (b) effective strain. Note that open and solid symbols have been taken from refs. [6] and [10], respectively.

More significant example is shown in Fig. 6. It is a tomographic image of fracture surface. The material is a 5154 aluminum alloy and its porosity was 0.32 %, while it is 0.20 % in the 2024 aluminum alloy shown in Fig. 5. This material has a pan-cake-like grain structure. Micro pores are aligned on grain boundaries. The tensile test of Fig. 6 was performed with the loading axis perpendicular to the aligned grain boundaries. As such, the majority of the fracture surface was covered by dimples that had been

controlling mechanical properties, and especially for improving the high-cycle fatigue properties.

### 3. Effects on mechanical properties

#### 3.1 Ductile fracture

The synchrotron X-ray microtomography was also used to observe the effects of hydrogen micro pores during deformation and fracture of a 2024 aluminum alloy. High-density micro pores were observed in the alloys even before loading. Since hydrogen micro pores are heterogeneously nucleated on particles, the pre-existing hydrogen micro pores and voids caused by damage cannot be distinguished from their morphology. Although porosity for the material was relatively low, extensive growth of pre-existing hydrogen micro pores have been observed during tension as is shown in Fig.5 [5]. The hydrogen micro pores started to grow from an early stage, while the ordinary damage initiation increased rapidly after plastic strain had been accumulated to some extent. Areal fraction of the dimple patterns originating from the pre-existing hydrogen micro pores was approximately 7 ~ 28 % on the fracture surface in this case.

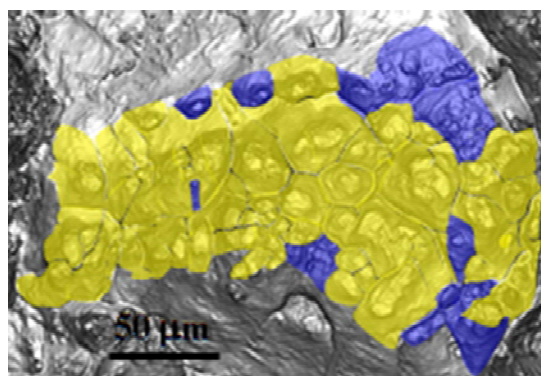


Fig. 6 3D perspective views of fracture surface of a 5154 aluminum alloy, representing the dimple pattern originated from hydrogen micro pores (painted in yellow) and that originated from particle damage (blue).

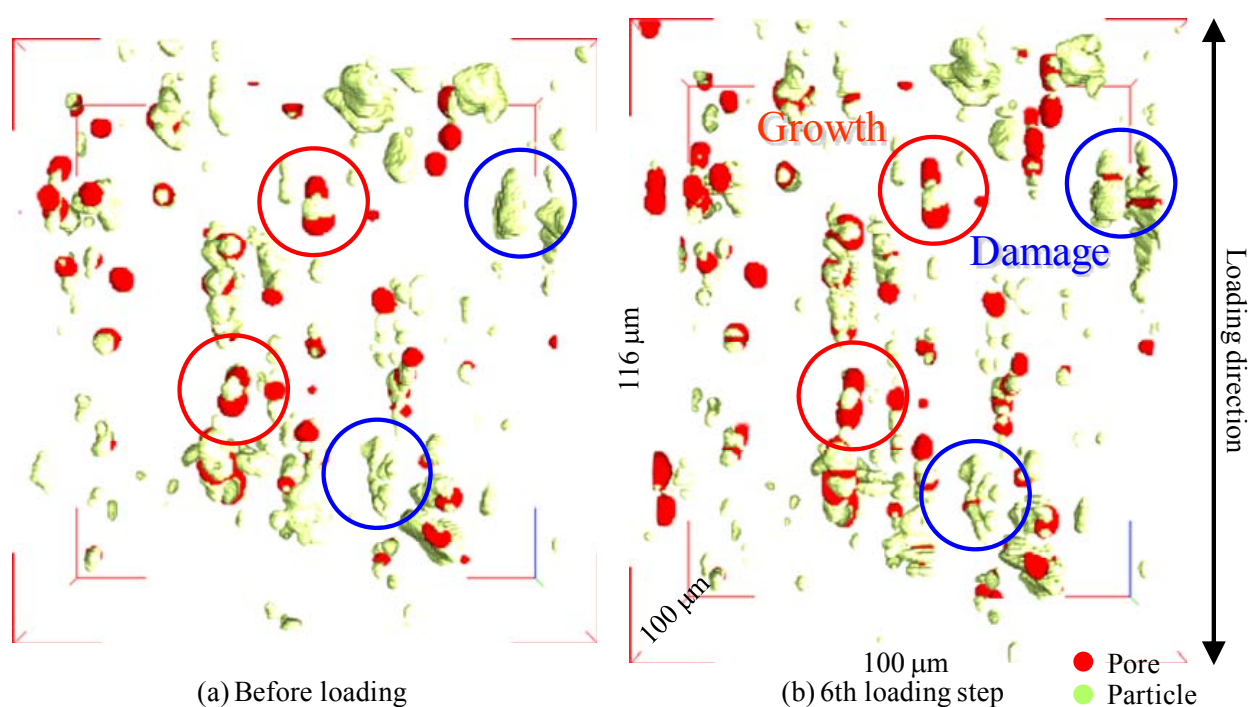


Fig. 5 3D perspective views of particles, pores and voids extracted from the tomographic volumes, representing competition of micro pore growth (highlighted with red circles) and void nucleation/growth (blue circles) during tension in a 2024 aluminum alloy.

originated from pre-existing hydrogen micro pores. It has been therefore concluded that the hydrogen micro pores more or less make contributions to ordinary ductile fracture, which has been overlooked to date.

Since the contribution of micro pores on mechanical properties was proved not to be neglectable, the necessity of a microstructural control, which is different from the currently available common knowledge, is suggested. For example, the conditions of high-temperature heat treatment such as homogenization and solution treatments should be controlled so that micro pore growth during the heat treatments should be taken into account. Subsequent metal working such as rolling and forging should also be properly controlled so that micro pores can be healed.

### 3.2 Fatigue fracture from micro pores

Usually, aluminum die-cast alloys have been used with casting surface. It can be assumed that defects exist in the sub-surface regions, which have been largely neglected in the conventional evaluations by removing the sub-surface regions before testing. Fatigue tests have been performed by the present authors using specimens with

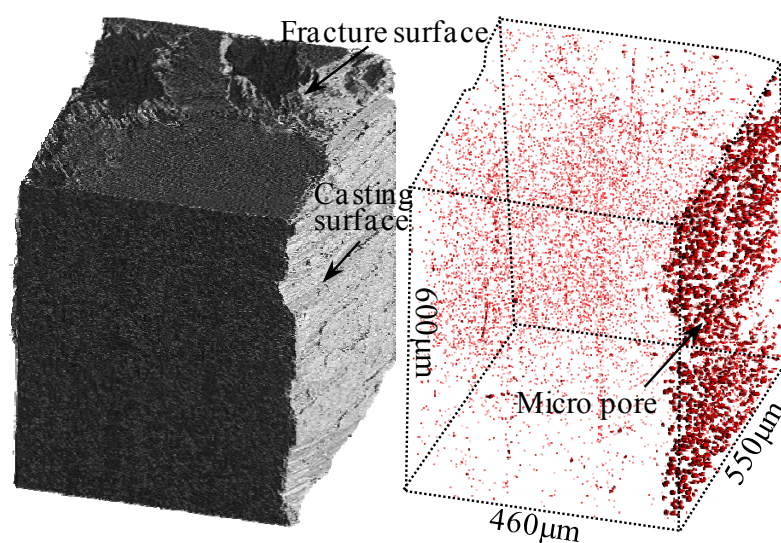


Fig. 7 A 3D perspective view of a fatigue specimen after fatigue fracture. The right image shows micro pores extracted from the tomographic volume.

casting surface. It has been revealed that specimens with shorter fatigue lives exhibited aligned micropores of approximately 10  $\mu\text{m}$  in diameter in a sub-surface region, which inevitably caused premature fatigue crack initiation. Fig. 7 shows a 3-D reconstructed image of a fatigue specimen after fatigue tests [2]. The material investigated was an Al-7%Si-0.35%Mg alloy that had been prepared through a high-quality die-casting technique. It is interesting to note that a high density of micro pores is observed beneath casting surface (with the distance of 30  $\mu\text{m}$  from the casting surface). In such a case, short fatigue lives are observed due to the existence of the micro pores. The existence of such agglomerated micro pores has not been reported to date, probably because of the difficulty in observing microscopic features in such vicinity of surface by means of the conventional metallographic techniques. The die-cast alloy had been tempered to T6 condition, including the high temperature exposure at 803 K for 5h during a solution heat treatment. As can be easily supposed from the previous section, significant growth of micro pores has been observed during the heat treatment, thereby inducing detrimental effects on the tempered alloy, and not so for as-cast alloys.

The in-situ observation clearly revealed fatigue crack initiation from agglomerated micropores. For example, Fig. 8 demonstrates fatigue crack initiation behavior from agglomerated micro pores [2]. In general, fatigue cracks are semicircular when the cracks are initiated from surface. On the other hand, the fatigue cracks observed in Fig. 8 are elongated parallel to the specimen surface, suggesting simultaneous crack initiation from plural crack initiation sites or predominant crack growth in the lateral direction after the fatigue crack initiation from a single crack initiation site. Anyway, it can be inferred that micro pores can significantly promote fatigue crack initiation and/or fatigue crack growth. The latter is evidenced by another research in which micro pores were found to be a preferential path for fatigue crack propagation [8]. Geometrical relationship between micro pores and a crack has been investigated, enabling modes I and II stress intensity factors calculated along the whole fatigue crack paths. Mode I stress intensity factor was found to increase significantly when a fatigue crack approaches a micro pore.

#### 4. Summary

High-density micro pores have been identified to exist in almost all kinds of aluminum alloys except pure aluminum owing to the recent development of the synchrotron X-ray microtomography. The X-ray microtomography technique is especially effective for micro pore observation, since micro pores are easily filled with abrasive powders during sample preparation processes for observation, such as cutting and polishing. This is the reason why such high-density micro pores had not been recognized until the

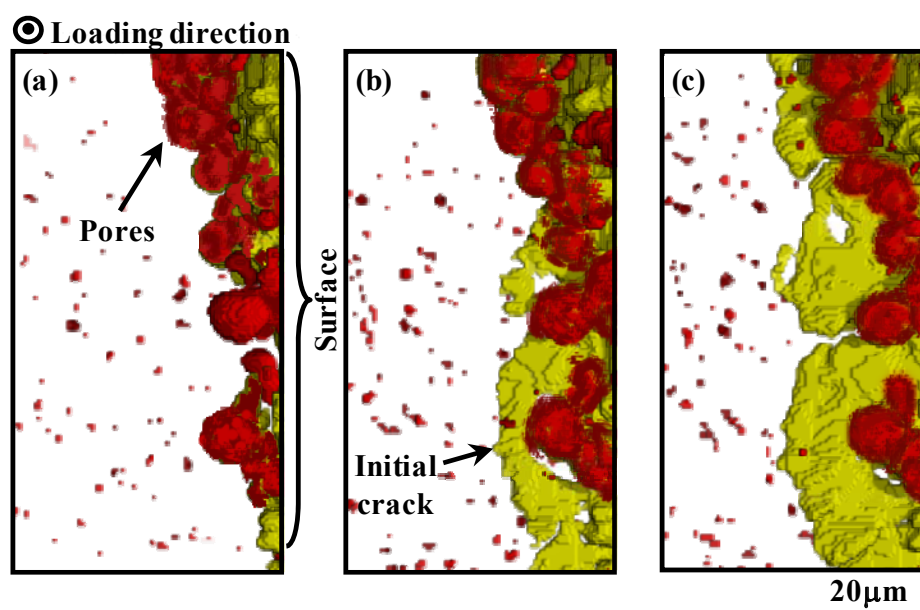


Fig. 8 In-situ observation of fatigue crack initiation from sub-surface micro pores. Micro pores are highlighted in red, and surface and a fatigue crack are highlighted in yellow. (a), (b) and (c) are captured at 0, 80,000 and 98,000 cycles, respectively.

synchrotron X-ray microtomography was applied. Formation, growth, shrink and annihilation behaviors of each micro pore are tracked during heat treatments, metal forming processes and external monotonic and cyclic loading. Mechanical and metallurgical conditions for the micro pore growth and closure have been clarified by means of the quantitative analysis of 3D images. It has been found that considerable amount of hydrogen contained in aluminum alloys is trapped in micro pores, while it is quite limited in a pure aluminum. It has been also clarified that there is a strong correlation between the local strain values with micro pore closure behavior.

The in-situ 3-D observations have clearly revealed that the existence of such micro pores sometimes strongly affects mechanical properties such as strength and fatigue. It is noteworthy that competitive growth between pre-existing high-density micro pores and voids originating from particle damage during loading, which is the conventional ductile fracture mechanism, was observed under tension. According to the estimation on the areal fraction of dimple pattern originating from the pre-existing hydrogen micro pores, it has been concluded that the hydrogen micro pores more or less make contributions to the ordinary ductile fracture at least to the unignorable extent. The observations do imply that it might overturn a well-established ductile fracture theory. Agglomeration of micro-pores in a sub-surface region observed in the heat-treated die-cast aluminum alloy would also be an important finding. It has been revealed that fatigue crack initiation is more apt to occur where micro pores are agglomerated. This may provide a new microstructural control method for the enhancement of fatigue resistance by controlling the size, density and spatial distribution of pores.

### Acknowledgements

The synchrotron radiation experiments were performed with the approval of JASRI through proposal numbers 2006A1056, 2007A1618 and 2007B1078. This work was undertaken as part of a Grant-in-Aid for Scientific Research (A) from the JSPS, as subject No. 20246102. The authors thank Dr. H. Tanaka in Sumitomo Light Metal Ind. Ltd. for providing materials used. One of the authors (HT) is also grateful for the support of the Light Metal Educational Foundation.

### References

- [1] G. Itoh, M. Kanno: *KINZOKU*, 66(1996), 599-610.
- [2] S. Masuda, H. Toda, S. Aoyama, S. Orii, S. Ueda and M. Kobayashi, *J. Japan Foundry Engineers Soc.*, 81(2009), 475-481.
- [3] H. Toda, T. Hidaka, M. Kobayashi, K. Uesugi, A. Takeuchi, K. Horikawa, *Acta Mater.*, 57(2009), 2277-2290.
- [4] H. Toda, I. Sinclair, J.-Y. Buffière, E. Maire, K. H. Khor, P. Gregson, T. Kobayashi, *Acta Mater.*, 52(2004), 1305-1317.
- [5] H. Toda, H. Oogo, K. Uesugi and M. Kobayashi, *Mater Trans*, 57(2009), 2285-2290.
- [6] H. Toda, K. Minami, K. Koyama, K. Ichitani, M. Kobayashi, K. Uesugi, Y. Suzuki, *Acta Mater.*, 57(2009), 4391-4403.
- [7] H. Toda, S. Sakaguchi, M. Kobayashi, K. Uesugi, Y. Suzuki, *Acta Mater.*, 58(2010), under review.
- [8] H. Zhang, H. Toda, H. Hara, M. Kobayashi, T. Kobayashi, D. Sugiyama and N. Kuroda, *Metall. Mater. Trans. A*, 38A(2007), 1774-1785.
- [9] J.H. O'Dette, *J. of Met*, 9(1957), 924.
- [10] H. Toda, T. Yamaguchi, M. Nakazawa, Y. Aoki, K. Uesugi, Y. Suzuki, and M. Kobayashi, *Acta Mater.*, 58(2010), in press.
- [11] M. Kobayashi, H. Toda, Y. Kawai, T. Ohgaki, K. Uesugi, D.S. Wilkinson, T. Kobayashi, Y. Aoki, M. Nakazawa, *Acta Mater*, 56(2008), 2167-2181.